Organic Electronics 102 (2022) 106429

Contents lists available at ScienceDirect

Organic Electronics

journal homepage: www.elsevier.com/locate/orgel

Impact of ferromagnetic electrode length and thickness on Magnetic Tunnel Junction-Based Molecular Spintronic Devices (MTJMSD)

Marzieh Savadkoohi, Christopher D'Angelo, Andrew Grizzle, Bishnu Dahal, Pawan Tyagi *

Center for Nanotechnology Research and Education, Mechanical Engineering, University of the District of Columbia, Washington DC, 20008, USA

ARTICLE INFO

Keywords:
MTJ
SMM
Ferromagnets
Molecular spintronics
Paramagnetic molecules

ABSTRACT

A knowledge gap exists about the impact of variation in length and thickness of ferromagnetic(FM) electrodes on molecular spintronics devices' ability to manifest molecular coupling impact. Magnetic Tunnel Junction-Based Molecular Spintronic Devices (MTJMSDs) are potential candidates for inventing highly correlated materials and devices and investigating the fundamental science of organic spintronics. This paper reports our experimental observations providing the dramatic impact of variation in ferromagnetic electrode length and thickness on paramagnetic molecule-based MTJMSD. Room temperature transport studies were performed to investigate the effect of FM electrode thickness. On the other hand, magnetic force microscopy measurements were conducted to understand the effect of FM electrode length extending beyond the molecular junction area, i.e., the site where paramagnetic molecules bridged between two FM. In the strong molecular coupling regime, transport study suggested thickness variation caused ~1000 to million-fold differences in junction conductivity. MFM study revealed near-zero magnetic contrast for pillar-shaped MTJMSD without any extended FM electrode. However, MFM images showed a multitude of microscopic magnetic phases on cross junction shaped MTJMSD where FM electrodes extended beyond the junction area. To understand the intriguing experimental results, we conducted an in-depth theoretical study using Monte Carlo Simulation (MCS) approach. MCS study utilized a Heisenberg atomic model of cross junction shaped MTJMSD to gain insights about room temperature transport and MFM experimental observations of microscopic MTJMSD. To make this study applicable for a wide variety of MTJMSDs, we systematically studied the effect of variation in molecular coupling strength between magnetic molecules and ferromagnetic (FM) electrodes of various dimensions. Our theoretical results suggest 25 atoms thick FM electrode show very weak molecular coupling impact and of the same order of experimentally studied FM electrode dimensions showing weak effect. Also, MCS results agree with experimentally observed multiple magnetic phases on lengthy FM electrodes of an MTJMSD.

1. Introduction

Electron spin-based molecular spintronics devices (MSDs) can be transformative for computer hardware and produce virtually infinite possibilities for discovering novel materials with intriguing phenomena [1–3]. Different techniques such as using a nanogap junction between ferromagnet (FM) electrodes (Fig. 1a) and sandwiching molecules between ferromagnetic electrodes (Fig. 1b) [3,4]to attach molecules are some of the major approaches used for fabricating MSDs [5]. These conventional MSD approaches successfully demonstrated the feasibility of the MSD concept. However, these approaches suffered from difficulties such as the little opportunity for mass production, extreme difficulty in using FM electrodes, damage to molecular channels during fabrication, atomic-level defects, etc. Additionally, understanding temperature-dependent MSD properties with complex single-molecule magnets (SMM) [6] like molecules and FM electrodes theoretically is a crucial roadblock in the designing process [5]. To resolve long-standing issues and to bring the advantages of commercially successful spintronics devices, magnetic tunnel junctions (MTJ) were used as a testbed (Fig. 1c) for making versatile and industrial fabrication friendly MSD (Fig. 1d) [7]. The development of MTJ based MSD (MTJMSD) also adds tremendous advancement opportunities for the MTJ research field as there are very limited FM electrode and insulator options [8–10]. Utilizing MTJ as a testbed for MSD fabrication can address the limitations of both MSD [11–13] and MTJ fields [5].

MTJMSDs are made of two FM electrodes that are separated by a

* Corresponding author.
E-mail address: ptyagi@udc.edu (P. Tyagi).

https://doi.org/10.1016/j.orgel.2022.106429
Received 29 October 2021; Received in revised form 19 December 2021; Accepted 2 January 2022
Available online 6 January 2022

nanoscale (~2 nm) thick insulator (Fig. 1c). In this approach, paramagnetic molecules are covalently attached to the exposed edges of FM electrodes in a cross-junction-shaped MTJ (Fig. 1d and e). Connecting a vast range of molecules to various FM electrodes can result in enormous MTJMSD possibilities, which can be extremely challenging to test experimentally (Fig. 1e). We conducted numerous control experiments, including reversing the effect of OMC and regaining tunnel junction current [14]. The strong exchange interaction between molecule's spin and FM electrode was observed to produce numerous intriguing experimental observations: current suppression [15], long-range ordering [16], and the spin photovoltaic effect [17]. MTJMSD also exhibited unstable million percent magnetoresistance [18], dramatically different from the typical few percent magnetoresistances observed on untreated MTJ testbed [15]. However, prior work did not explore the influence of FM electrode thickness and length on the futuristic MTJMSD properties. This paper provides experimental insights into the effect of FM electrode thickness and length on transport and magnetic ordering. To provide insights into the mechanism, we report Monte Carlo simulations on the representative Heisenberg model representing the cross-junction shaped MTJMSD-utilized in the experimental studies.

2. Experimental details and simulation methodology

The MTJ were patterned and deposited on silicon (Si) substrate with ~300 nm silicon dioxide layer. The bottom electrode was photolithographically defined to be ~5 μm wide channel (Fig. 1f). For producing a difference in magnetic hardness of the top and bottom electrodes, the bottom electrode was deposited as a bilayer of ~ 5–7 nm cobalt (Co) and 3–5 nm NiFe. A ~5 nm tantalum(Ta) seed layer was used for promoting adhesion between Co and the insulating substrate. For making a cross-junction-shaped tunnel junction, photolithography was performed to yield ~5 μm width channel (Fig. 1g). In the photoresist cavity sequentially, a 2 nm thick alumina (AlOx) (Fig. 1h) and a ~10 nm thick NiFe top electrode (Fig. 1i) were deposited. It is noteworthy that the second photolithography played two crucial roles. Utilization of the same photoresist cavity for all further depositions ensured that the top electrode and aluminum oxide have the exact lateral dimensions; this provision ensured that minimum physical separation between the top and bottom electrode would be equal to insulating thickness. Additionally, the photoresist can be easily removed during the liftoff process to provide clean edges for bringing molecules of interest in the contact of two metal electrodes. The liftoff was accomplished to remove excess materials and produce a cross-junction shaped Ta/Co/NiFe/AlOx/NiFe MTJ with exposed side edges (Fig. 1g). Along the exposed side edges, organometallic molecular clusters (OMCs) (Fig. 1b) [19] were bridged across the AlOx to complete the MTJMSD fabrication. In-depth details about OMCs properties in an as-produced state are published elsewhere [19,20]. To study the effect of paramagnetic molecules on MTJ without any extended ferromagnetic electrode, we also produced a pillar-shaped tunnel junction. Pillar-shaped Ta/Co/NiFe/AlOx/NiFe tunnel junctions were produced via sequential deposition of all the layers in a single photoresist cavity.

As the last fabrication step, the paramagnetic molecules were covalently bonded between the two ferromagnet electrode on completed cross-junction and pillar-shaped MTJ to produce MTJMSD. For this study, we utilized OMCs. The process details of connecting OMCs to metal electrodes were published elsewhere [16,17]. We utilized an electrochemical process for molecular self-assembly that is known to produce good metal-thiol bonding in few minutes [21,22]. An OMC possessed cyanide-bridged octametallic molecular cluster, $[(pzTp)Fe^{III}(CN)_3]_4[Ni^{II}(L)]_4[O_3SCF_3]_4$ [(pzTp) = tetra(pyrazol-1-yl)borate; L = 1-S(acetyl)tris(pyrazolyl)decane] chemical structure [19]. The internal exchange coupling between metallic ions in the OMCs exhibited S = 6 spin state in the bulk powder form at <10 K [19]. It is extremely challenging to determine the actual OMC spin state when covalently bonded between two ferromagnetic electrodes in an MTJMSD. However, room temperature observations of spin-photovoltaic effect, current suppression, and other phenomena assert that OMC could maintain a net magnetic spin state at room temperature. We have investigated the transport and magnetic properties of MTJMSD, and experimental details are published elsewhere [15–18].

Our MTJMSD fabrication process produced strong bonding between the spin state of the molecule and the NiFe FM electrode. NiFe electrode possesses thermodynamically stable unoxidized Ni that is available to covalently bond with the help of thiol functional groups present at end alkane tethers of OMC. Alkane tether is endowed with low hyperfine splitting and spin scattering [23–25]to enable strong coupling between FM electrode and spin state of OMC. The conceptual figure defined OMC exchange coupling with top and bottom electrodes with J_{mL} and J_{mR} exchange parameters (Fig. 1e).

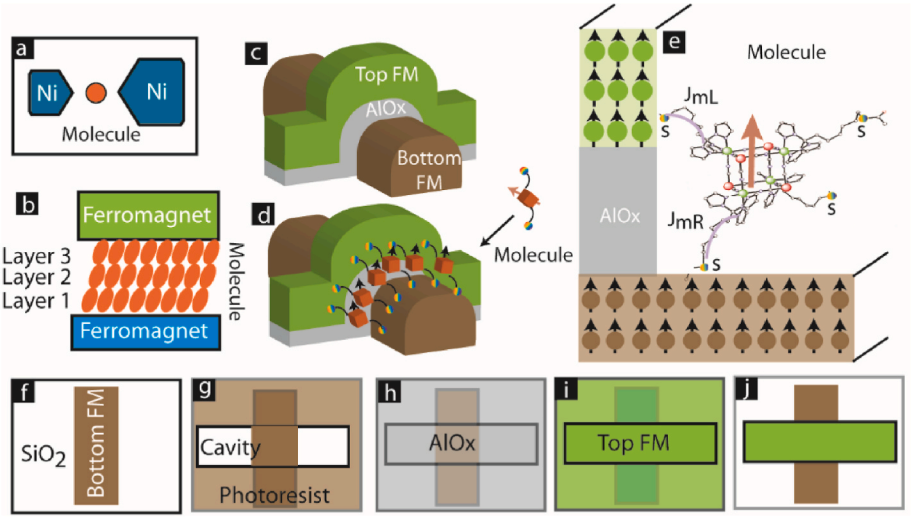

Fig. 1. Conceptual representation of conventional (a) nanpgap breakjunction, and (b) sandwiched type MSD. MTJMSD 3D-architecture (c) before and (d) after magnetic molecules treatment (e) 3D MTJMSD model analogs to MTJMSD in panel (d). MTJMSD fabrication flow is based on (f) depositing bottom electrode in photolithographically defined cavity, (g) pholollithography for (h) AlOx insulator, (i) top electrode. (j) Liftoff producing exposed edge MTJ.

3. MCS methodology

To investigate the atomic-scale mechanism of the effect of FM electrode dimensions, we conducted Monte Caro Simulation (MCS). MCS theoretical investigation of MTJMSD considered several variables such as molecular coupling to individual FM electrodes, thermal energy, molecular spin state, the impact of competing coupling via tunnel barrier and molecules, etc. It is noteworthy that conventional DFT approaches are limited to zero temperature and the specific configuration of molecular channels and ferromagnetic electrodes [26–30]. DFT studies are also challenging for large device sizes and often require various approximations, and are performed with a single FM electrode only [26–30]. To tackle this problem of understanding experimental MTJMSD attributes arising due to variation in FM electrode width and thickness, we conducted extensive MCSs. For MCS, we have utilized the Heisenberg model of MTJMSD. In the Heisenberg model, two 3D FM electrodes were placed at 90°. Paramagnetic molecules' placement around the tunnel junction perimeter [15,17,31] was represented by a 5 × 5 dimension hollow molecular rectangle and placed between the FM electrodes (Fig. 1c). Dimension of FM electrode was changed based on the number of atoms along the length, and thickness dimensions and width were fixed to be five atoms. Typically FM electrodes had 50 atom length, five atom thickness, and five atom width. For investigating the effect of length, the length of FM two electrodes was varied in the step of 50 while keeping thickness and width at 5. For exploring the effect of thickness, the thickness of two FM electrodes was varied in the step of 5 while maintaining length fixed at 50 and width at five atomic units.

To achieve the equilibrium energy state, we used the continuous Metropolis algorithm and Markov process to minimize the energy of the Heisenberg model in eq. (1) [32].

Here, J_L and J_R are inter-atomic exchange couplings in the left and right electrodes, respectively. S_i is the 3D spin vector of atoms in FM electrodes and molecules. Molecule internal exchange coupling factors (J_{OMC}) and anisotropy(D_{OMC}) were fixed to result in the paramagnetic state with fixed spin. We varied the exchange coupling strengths and nature between the paramagnetic molecule and left FM electrode (J_{mL}) and right FM electrode (J_{mR}). Fig. 1e provides a physical representation of J_{mL} and J_{mR} in MTJMSD. For this study, thermal energy (kT) was set to 0.1 to encompass near room temperature characteristics of FM electrodes. For ensuring that each MCS reached an equilibrium state, ~200 M to 2 Billion iterations were performed. We studied the spatial and temporal evolution of MTJMSD's magnetic moment (M) and FM electrodes as a function of length, thickness, and molecular coupling J_{mL} and J_{mR}. More details about the MCS are published elsewhere [33].

4. Results and discussion

4.1. Experimental results

We conducted a transport study to investigate the effect of ferromagnetic electrode thickness. For this study, MTJMSD were fabricated with ~10 nm thick Co/(5 nm)/NiFe(5 nm) and ~20 nm thick Co/(15 nm)/NiFe(5 nm) bottom electrodes. A bare MTJ produced with a 10 nm thick bottom electrode exhibited a clear tunneling current. Bridging of ~10,000 OMC produced a strong impact on the magnetic ordering of the ferromagnetic electrodes at room temperature. The highest current level seen on the MTJ with OMC was ~4 μA for ~100 mV (Fig. 2a). Interestingly, MTJMSD with 10 nm bottom electrode settled in a suppressed current state in the nA range at room temperature (Fig. 2b). This

$$E = -J_L\left(\sum_{i\in L}\vec{S}_i\vec{S}_{i+1}\right) - J_R\left(\sum_{i\in R}\vec{S}_i\vec{S}_{i+1}\right) - J_{mL}\left(\sum_{i\in L, i+1\in mol}\vec{S}_i\vec{S}_{i+1}\right) - J_{mR}\left(\sum_{i-1\in mol, i\in R}\vec{S}_{i-1}\vec{S}_i\right) - J_{OMC}\left(\sum_{i-1\in mol, i\in R}\vec{S}_{i-1}\vec{S}_i\right) - D_{OMC}\left(\sum_{i\in L}\vec{S}_i^2\right) \quad (1)$$

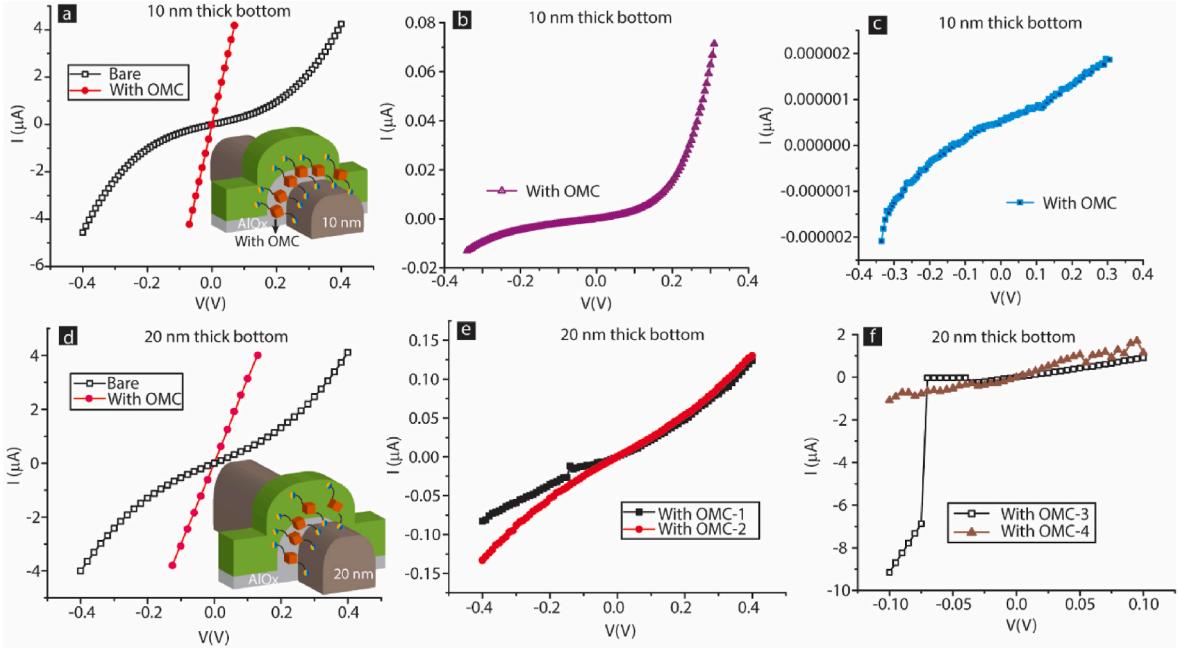

Fig. 2. MTJMSD with 10 nm bottom electrode showing (a) tunneling transport on bare MTJ and the highest current value observed, (b) asymmetric nA range suppressed state, (c) pA level suppressed current state. MTJMSD with ~20 nm thick bottom FM electrode showing (d) tunneling transport on bare MTJ and the highest current value observed, (e) nA range suppressed state, and (f) instability leading to high and low current state.

MTJMSD further stabilized into pA level suppressed current state at room temperature (Fig. 2c). Generally, nA to pA order suppressed current state remained stable at room temperature for the lifetime of the sample and was observed for over >24 months. The bare MTJ and OMC molecule-induced data is symmetric in Fig. 2a. It is presumably due to a similar density of states profile near the Fermi energy of two ferromagnetic electrodes [8]. The transport data due to OMC channels in Fig. 2a was captured soon after forming the molecular bridges when MTJMSD was still in the early stage. In the initial state MTJMSD's are still in the early stage of magnetic moment settlement leading to typically symmetric I–V. We observed that molecule-induced long-range impact on magnetic electrodes requires a few hours [15]. On the other hand, as OMC-induced long-range ordering progressed and stabilized into a spin-polarized state [15], two magnetic electrodes started attaining dramatically different magnetic ordering and phases. MFM data discussed in Fig. 3 in this paper provides vivid observations of OMC impact on FM electrodes. The asymmetric I–V in Fig. 2b and c corresponds to the difference in ferromagnetic electrode properties arising due to OMC-induced spin filtering and higher spin polarization [16]. Extensive discussion about the correlation of different current states and OMC molecule-induced magnetic phases are also discussed elsewhere [15,16]. This 10 nm thick bottom electrode-based MTJMSD also exhibited many intriguing phenomena, such as the spin-photovoltaic effect [15–18]. Multiple magnetic studies suggested the OMC dramatically impacted ferromagnetic electrodes.

According to prior work, covalently bonded OMC channels resulted in spin filtering effect [34,35], leading to antiferromagnetically aligned ~100% spin-polarized electrodes on MTJMSDs [18]. In this OMC-induced magnetic electrodes state and antiparallel alignment [32], transport is blocked via molecules and tunnel barrier both [18], and suppressed current appears (Fig. 2c). In the resistor-like high current state, MTJMSD transport is dominated by OMC channels serving the roles of an electrical short circuit along the side edges (Fig. 2a). We are unable to provide a precise description of the electrodes' magnetic state because MTJMSD's high current state is short-lived due to time-dependent equilibration; MTJMSD's high current transcended to a low current state [16]. OMC molecules really dominate over tunnel barrier can also be observed from the prior studies where paramagnetic tantalum [14] metal electrodes were employed. OMC connected to tantalum metal electrodes in the same cross-junction-shaped device geometry as discussed here produced a stable current increase above the leakage current level that was observed on bare tunnel junction. Simmons tunneling model [36] was applied on transport data before and after OMC channel formation [14]. Simmons's model [36] suggested that barrier thickness reduced from ~2.4 nm (AlOx insulator thickness) to 10 carbon alkane tether length connected to OMC core [20]. In this case, the charge moves from the electrode to the OMC core via one alkane tether and leaves on to another electrode via the second tether-this arrangement is equivalent to a double barrier tunnel junction [14]. We believe that in a high current state, the net transport in the present device geometry is due to both OMC channels and tunnel barrier's contribution. However, OMC channel contribution is much more than tunnel barrier (Fig. 2a). We also conducted control experiments where the molecular channel role was reversed by breaking the OMC -metal electrode bonds [14]. We do not claim to be aware of all the aspects of transport and actively designing experiments by employing different types of molecules [31] as transport channels under our ongoing and future studies.

Interestingly, for ~20 nm thick bottom electrode, we observed OMC effect was significantly different. OMC produced a high current state on MTJ in the initial state (Fig. 2d) and was similar to that of MTJ with a 10 nm thick bottom electrode (Fig. 2a). OMC was able to produce a modest

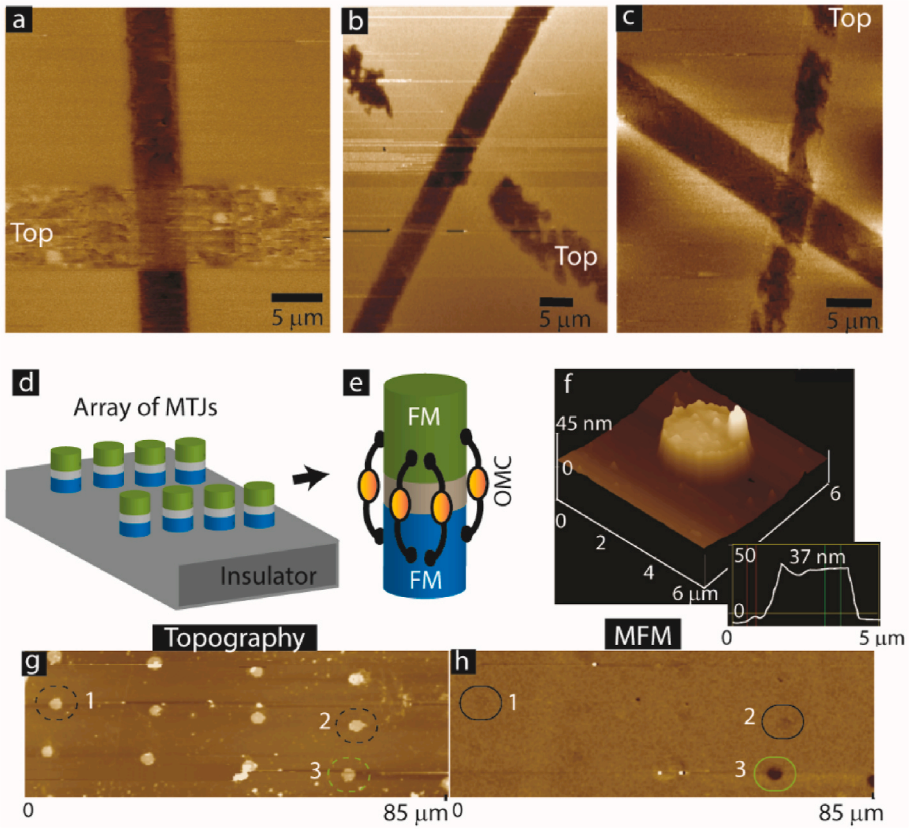

Fig. 3. MFM of 10 nm thick bottom electrode based MTJMSD showing (a) high contrasting top and bottom FM electrodes, (b)disappearance of magnetic phase near junction, (c) sporadic high and low magnetic contrast regions. Cartoon of (d) array of pillar shaped MTJs (e) each will host OMCs along the side edges. Topography of (f) single MTJMSD pillar and (g) multiple MTJMSD. (h) MFM of OMC impacted MTJs MFM adopted from ref 16.

metastable current suppression. We observed rather symmetric ~10 nA level current suppression at ~100 mV (Fig. 2e). However, a pA level suppressed state could not be observed. Many times repeating I–V studies caused a sudden change in transport (Fig. 2f). In summary, MTJMSD with thicker electrodes showed unstable suppressed current states at room temperature. It is intriguing how doubling the thickness yielded an unstable I–V response as compared to the 10 nm FM electrodes case discussed in Fig. 2b and c. Our prior work showed that FM/OMC coupling is based on extremely strong Ni–S covalent bonds [37]. Such Ni–S covalent bonds are air-stable even at high temperatures [37]. However, strong OMC-induced strong exchange coupling struggled to produce a stable impact on 20 nm thick FM electrodes and prompted us to conduct theoretical simulation for atomistic understanding. As discussed elsewhere, Monte Carlo Simulation showed that increasing thickness reduced the magnetic molecule impact on the full thickness of the FM electrode. Molecule strong exchange coupling impact was strong in the vicinity of the molecular junction and decreased rapidly with increasing thickness. Some portions of thick FM electrodes, away from the molecular junction area, assumed incoherent and somewhat random magnetic states that presumably caused unstable I–V response (Fig. 2f).

We also studied the effect of the length of ferromagnetic electrodes. For this study, we conducted a magnetic force microscopy (MFM) study. The experimental details are published elsewhere [16]. For this study, the top and bottom electrodes were ~10 nm thick. MFM study of bare MTJ generally yielded identical phase colors. However, OMC treated cross junction showed intriguing long-range interactions. In the nA to pA range, current suppression states corresponded to MFM images in Fig. 3a and b. However, in the transient state, a magnetic phase appeared randomly (Fig. 3c). Here, we do not assert that each MFM image can be reproduced in the exact same form. MTJMSD state at the time of experimentation governs the nature of MFM data. However, MFM data informs that the OMC effect spread far beyond the junction area. Also, a major impact was observed on the top electrode. Since we only conducted qualitative MFM studies, we are not sure the bottom electrode also changed significantly in a manner that could not be discerned from the MFM data. To further investigate the effect of MTJMSD without extended FM electrodes beyond the junction area, we produced pillar-shaped MTJs. An array of several thousand MTJ was produced (Fig. 3d). Each of the MTJ pillars was transformed in the molecular device by bridging the OMC channels along the junction perimeter

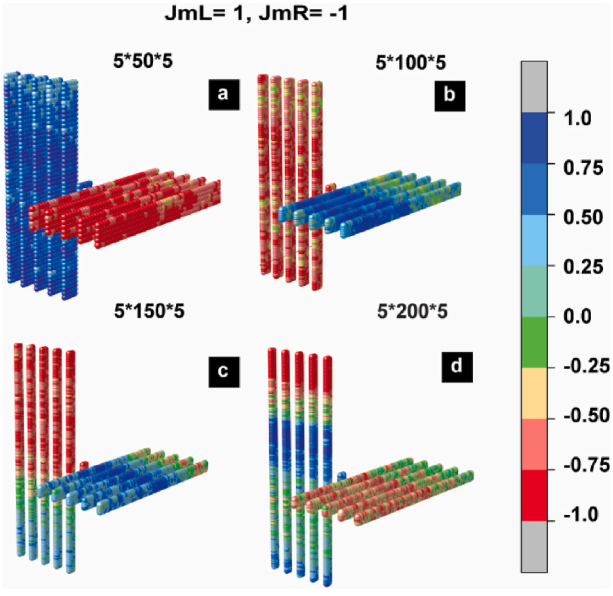

Fig. 4. 3D Lattice plot of MTJMSD′ s Magnetic Moment when JmL = 1 and JmR = −1 for increased length devices (a) 5*50*5, (b) 5*100*5 (c) 5*150*5 (d) 5*200*5.

(Fig. 3e). AFM thickness measurement was conducted to check the structural integrity of MTJMSD pillars (Fig. 3f). We found that OMC did not impact pillars structurally, and the presence of the MTJ array could be noticed from the topography (Fig. 3g). Interestingly, the MFM of the MTJMSD pillar did not produce any measurable contrast (Fig. 3h). Circled areas 1 and 2 in the MFM image point to the location of MTJMSD with negligible phase contrast. Circled area 3 indicates an MTJ that could not be transformed in MTJMSD and exhibited a high magnetic difference (Fig. 4h). It appears that OMC impact significantly differed for MTJMSD with extended electrodes (Fig. 3a–c) versus pillar-shaped MTJs (Fig. 4h).

The effect of thickness variation was significant on MTJMSD transport properties. As discussed in our prior publication [15], OMC channels covalently connected to ~ 10 nm thick ferromagnetic electrodes produced stable current suppression. In the early settlement state, a transient magnetoresistance (MR) was observed on MTJMSD; MTJMSD's unstable MR was estimated to be several thousand percent. Interestingly, bare MTJ exhibited ~17% MR MTJ [15], which is consistent with the typical order of MR observed on AlOx based MTJ [9]. Hence, OMC made a significant impact and transformed MTJ's properties. In the stable current suppression state, MTJMSD did not exhibit a magnetoresistance phenomenon. It is presumably due to the fact that OMC induced strong antiferromagnetic coupling between two FM electrodes of ~10 nm thickness. The OMC-induced coupling was too strong to overcome by the highest magnetic field we applied [32]. It is noteworthy that MR is only seen when one can align two FM electrodes parallel and antiparallel with respect to each other [38]. We could not overcome molecule-induced exchange coupling up to a 3T magnetic field (please see SQUID magnetization curve in Ref. [32]). For the 20 nm thick bottom electrode, MTJMSD was always in an unstable state. In this state, no stable transport characteristics or magnetoresistance were observed. The reason for unstable 20 nm thick MTJMSD is explained via the MCS data elsewhere in this paper. Also, the spin photovoltaic effect was observed on a 10 nm thick bottom electrode [17]. Extensive details about the spin photovoltaic effect have been discussed in a recent publication [17]. The 20 nm thick ferromagnetic electrode-based MTJMSD did not show any spin photovoltaic effect. Due to resource limitations, we were unable to systematically change the length of FM electrodes in our experiments to investigate the impact of length on MTJMSD's MR and spin photovoltaic effect. As shown in Fig. 3a vs. Fig. 3h, OMC could always impact ~10 nm thick FM electrodes near molecular junctions irrespective of length. The impacted FM electrode resulted in a spin photovoltaic effect. Future studies are in order where different molecular junction areas and lengths are to be investigated.

Our prior MCS study provided mechanistic understanding showing that the magnetic moment of the two FM electrodes aligned antiparallel to each other [32]. Our experimental SQUID magnetometry and ferromagnetic resonance corroborated with the MCS results [32]. There was a knowledge gap about the effect of FM electrode length and thickness for the cross-junction shaped MTJMSD when the molecule produced strong antiferromagnetic coupling. The case of molecule-induced strong antiferromagnetic coupling is especially important because of its direct relation with current suppression reported in Fig. 3. To investigate molecule-induced strong antiferromagnetic exchange coupling impact in the MCS study, we fixed J_{mL} and J_{mR} to ferromagnetic(+sign) and antiferromagnetic(- sign), respectively.

4.2. MCS size effect on MTJMSD's magnetic properties

To understand the length and thickness effect mechanism, we conducted an MCS study by varying the FM electrode length and thickness, while 16 molecular analogs were used in all studies. If two electrodes aligned perfectly antiparallel due to strong antiferromagnetic coupling, an MTJMSD will show near-16 magnetic moment. On the other hand, if multiple magnetic phases evolve within FM electrodes and around the junction due to increased length or thickness, the overall magnetic

moment will vary between the lowest and highest magnetic moment. To investigate the effect of device size on MTJMSD evolution to the equilibrium state, we ran MCS simulation in 200 Million $\leq$ iterations$\leq$ 2 Billion range. To compare the MTJMSD evolution at the same time scale, we compared data for 2 billion iterations. To investigate the strong molecule-induced coupling effect, we fixed ferromagnetic coupling between molecules with one FM electrode ($J_{mL} = 1$) and antiferromagnetic coupling with another FM electrode ($J_{mR} = -1$). This selection of J_{mL} and J_{mR} was inspired by our previous experimental work providing evidence of strong molecule induced strong antiferromagnetic coupling [32].

To analyze the effect of increasing length and thickness of the FM electrodes at the atomic level, we plotted spin vectors along the stable direction for the complete Heisenberg model (Figs. 4 and 5). Figs. 4 and 5 show 3D-lattice plots of different MTJMSD sizes in the direction where stabilization happened. The MTJMSD magnetic moment at each atomic site varies between −1 and 1, as shown in the color bar. As the results imply, up to ~50 atom long FM electrode, molecules can induce strong antiferromagnetic coupling between FM-electrodes for $J_{mL} = 1$ and $J_{mR} = -1$ (Fig. 4a). Molecular coupling impact appears to persist for MTJMSD with 100 atom long FM electrodes (Fig. 4a). Further increase in MTJMSD length resulted in multiple magnetic phases on the FM electrodes (Fig. 5c and d), as represented by the color stripe formation and more metastates within FM electrodes. MTJMSD with 150 atom long FM electrode exhibited both electrodes with multiple magnetic phases (Fig. 4c). The MTJMSD with 200 atoms long FM electrode showed multiple regions (Fig. 4d). It is apparent that molecules have reinforced a variety of magnetic phases near and far sections of FM electrodes. In this case, the net MTJMSD magnetic moment at the end of the simulation is expected to be significantly higher for the more extended FM electrode than the case when two FM electrodes are well aligned in the opposite direction (Fig. 4a). This result is consistent with what was observed earlier in temporal evolution plots. MTJMSD with length >100 does not reach ~ zero magnetic moment. In other words, molecules act strongly around the cross-junction area and lose their grip over the extended portions of the electrodes.

Fig. 5 shows the spatial orientation of magnetic moment with increasing device thickness. Interestingly, the impact of strong antiferromagnetic coupling is observable in all cases (Fig. 5). Two five atom thick FM electrodes were antiparallel with respect to each throughout the length (50 atoms), width(5 atoms), and thickness (Fig. 5a). However, as thickness increased presence of phases with incoherent spins increased. For example, the green color phase representing 0 to −0.25 spin was present in the ordered red color phase with −1 to −0.75 spin phases for the ten atom thick FM electrodes (Fig. 5a). The magnetic phases for 15 atoms thick FM electrode also showed incoherent spin phases (Fig. 5b). However, it is inconclusive if there were a significant difference with respect to the ten atoms thick FM electrode. For the 20 atoms, the thick FM electrodes area of incoherent phases increased remarkably (Fig. 5c). The MTJMSD with 25 atom thick FM electrodes exhibited dominance of incoherent phases (Fig. 5d). The 25 atom thick FM electrodes also showed that incoherent phases, low spin phases, were dominant away from the junction (Fig. 5d).

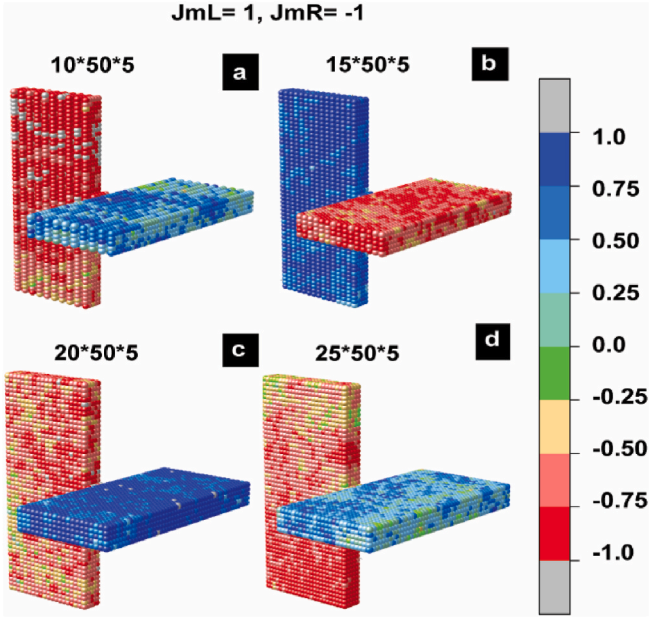

Fig. 5. 3D Lattice plot of MTJMSD′ s Magnetic Moment when JmL = 1 and JmR = −1 for increased thickness devices (a) 10*50*5, (b) 15*50*5 (c) 20*50*5 (d) 25*50*5.

Molecule-induced antiferromagnetic coupling effect on FM electrodes with different dimensions varied significantly. We quantify the impact of the molecular exchange coupling effect with the thickness and length of the FM electrode. For quantification, we shrunk the width dimension by taking an average of the FM atom's magnetic moment. We formulated a spatial correlation factor C to quantify the relationship between the spin direction of MTJMSD's paramagnetic molecules and FM electrodes. This factor C was calculated by computing the dot product between the average local spin of the FM electrode and the average spin of paramagnetic molecules (Eq. (2)).

$$C = (S_m \vec{x} + S_m \vec{y} + S_m \vec{z}).(S_{FM} \vec{x} + S_{FM} \vec{y} + S_{FM} \vec{z}) \quad (2)$$

Fig. 6 demonstrates a magnetic correlation between two FM electrodes and paramagnetic molecules in three device sizes. Here we have only focused on the MTJMSD with FM electrodes with 50 atom length and 5 atom thickness, 200 atom length and 5 atom thickness, 50 atom length, and 25 atom thickness (Fig. 6). In all the cases in Fig. 6, the width of FM electrode was fixed to be 5 atoms. As the results imply, the antiferromagnetic coupling has been induced between FM electrodes in all device sizes despite increasing length and thickness. The C correlation value varies between −1 and 1, where −1 shows a strong antiparallel correlation and 1 represents a parallel correlation between FM and molecule. For the MTJMSD with FM electrodes of 50 atom length and 5 atom thickness, the spatial range of molecule impact was throughout the length and thickness (Fig. 6a). However, for the MTJMSD with 200 atom length and 5 atom thickness, an FM electrode exhibited multiple correlated phases (Fig. 6b). Phases near molecular junctions were more correlated than those present toward the end. However, multiple disjointed yet equally correlated phases were observed. For example, the left side electrode showed a highly correlated phase near the junction. Another correlated phase towards the lower end was separated from the junction area by a less correlated phase (Fig. 6b). The effect of increasing thickness produced an entirely different impact on molecule correlated phases. Factor C was computed for increasing the FM electrode thickness. With MTJMSD with FM electrode of 50 atom length and 25 atom thickness, strongly correlated phases were localized around the junction area (Fig. 6c). Moving away from junction C was ~0.6. However, moving away along the length direction, C further decreased to 0.4 or lower. This result suggests that increasing thickness enables the creation of a gradient in molecule induces correlated magnetic phases. The long-range molecule-induced correlated phases are in close agreement with MFM data showing OMC-induced correlated phases.

We also investigated the effect of molecular coupling strength on the spatial impact range. For this study, we computed MTJMSD magnetic moment as a function of the J_{mL} and J_{mR} (Figs. 7 and 8). To assess the effect of different coupling strengths and natures, we varied molecular coupling strengths between −1 and 1 with a step of 0.1 in all device sizes. We conducted 441 simulations for each device size. Fig. 7 show the effect of variation in FM electrode length while width and thickness were fixed at 5 atomics units. The MTJMSD magnetic moment for 5 atoms thick and 50 atoms long FM electrodes showed that the opposite

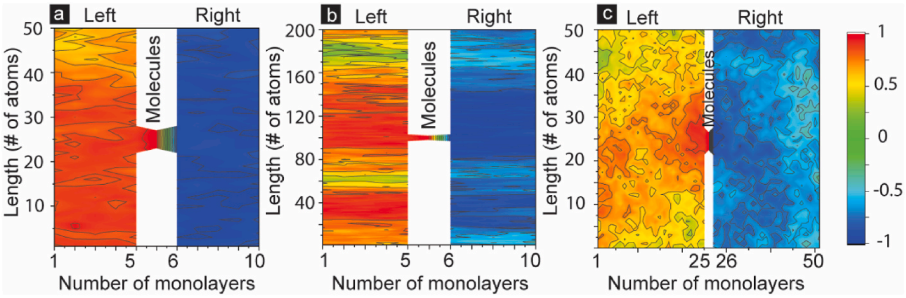

Fig. 6. Correlation factor contour plots of MTJMSD for all layers of left and right FM electrodes and the magnetic molecule when $J_{mL} = 1$, $J_{mR} = -1$, for device with FM electrodes of (a) 50 atom length and 5 atom thickness, (b) 200 atom length and 5 atom thickness (c) 50 atom length and 25 atom thickness. Width of FM electrode was 5 atom.

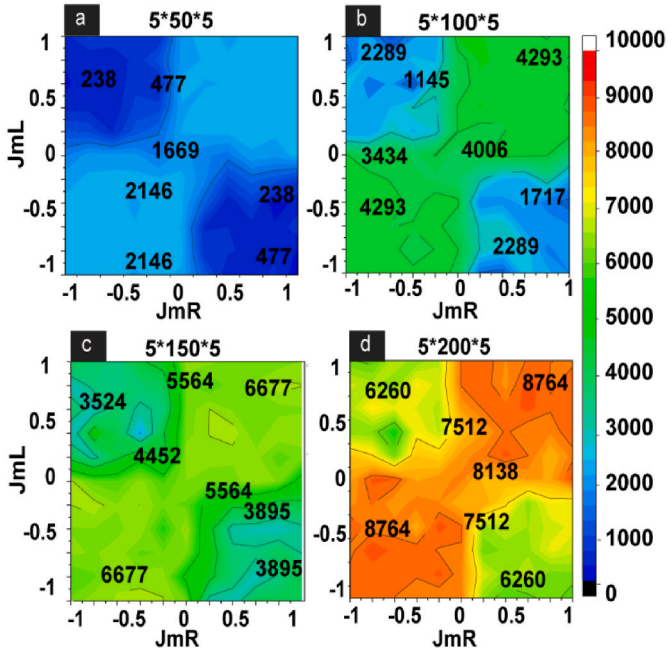

Fig. 7. Total MTJMSD's Magnetic Moment for increased length devices (a) 5*50*5, (b) 5*100*5 (c) 5*150*5 (d) 5*200*5.

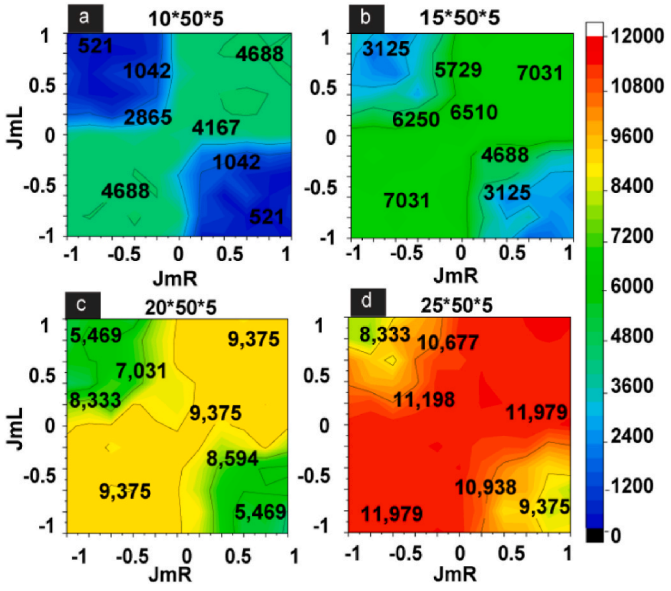

Fig. 8. Total MTJMSD's Magnetic Moment for increased widths devices (a) 10*50*5, (b) 15*50*5 (c) 20*50*5 (d) 25*50*5.

sign of J_{mL} and J_{mR} magnetic moment stabilized ~200 magnitudes; however, for the same sign, J_{mL} and J_{mR} led to net MTJMSD's magnetic moment ~2100 (Fig. 7a). It is noteworthy that in the case of molecule-induced ferromagnetic coupling, two short-length FM electrodes can be aligned parallel to each other, leading to a maximum of 2266. However, since MCS is conducted at $kT = 0.1$ and hence thermal energy may contribute to creating significant fluctuations. Similarly, the lowest magnetic moment of MTJMSD, i.e., 16, is possible for short-length FM electrodes. Due to thermal energy-induced disorders, the lowest magnetic moment could not be possible.

Interestingly, we observed that there existed a critical amount of J_{mL} and J_{mR} where the major transition occurs from a high to low magnetic moment state (Fig. 7a). This transition happens when molecular coupling strengths of one kind are too weak to control the large area FM electrodes. Furthermore, increasing the FM electrode length to 100 atoms made it difficult to stabilize low magnetic moment for the antiferromagnetic molecular coupling where J_{mL} and J_{mR} were of opposite sign (Fig. 7b). The central region turned into a high magnetic moment state (Fig. 7b). It must be noted that a large number of phases are possible for the antiferromagnetic molecular coupling regions. The existence of various molecule-induced phases is evident from the multiple regions associated with opposite signs of molecular coupling. For the case of 150 atom long FM electrode, the contour plot was similar to that of 100 atoms long FM electrode MTJMSD (Fig. 7c). For the case of 200 atom long FM electrodes, the regions associated with molecule indicated antiferromagnetic coupling and ferromagnetic coupling were very close in magnitude (Fig. 7d). Roughly, the ratio of low to high magnetic moment regions for 50,100, 150, and 200 atom long FM electrodes were ~0.1 (Fig. 7a), 0.4 (Fig. 7b), 0.5 (Fig. 7c), and 0.7 (Fig. 7d), respectively.

We also investigated the effect of variation in molecular coupling strength as a function of FM electrode thickness. FM electrode width and length was fixed to be 5 and 50 atomic unit, respectively. For 5 atom thick FM electrode contour plot is shown in Fig. 7a. Increasing the FM electrode thickness to 10 atoms created clear contrasting high and low magnetic regions (Fig. 8a). However, it is apparent that stronger molecular coupling is needed to produce a low magnetic moment state (Fig. 8a) compared to MTJMSD with a smaller thickness electrode (Fig. 7a). Furthermore, increasing FM electrode thickness to 15 atoms reduced the difference between the high and low magnetic moment states for ferromagnetic and antiferromagnetic coupling (Fig. 8b). For 20 atom thick FM electrodes, MTJMSD showed more constricted low

magnetic moment and smaller differences in low and high magnetic moment states (Fig. 8c). Interestingly, for the 25 atom thick FM electrodes, a high magnetic moment state persisted for most of the combination of the J_{mL} and J_{mR} (Fig. 8d). The contour plot shown in Fig. 8d is congruent with the 3D Heisenberg model, showing the molecule's effect for the thick electrodes are confined near the junction and exhibit a gradient effect. The ratio between high and low magnetic moment for 5,10,15,20, and 25 atom thick FM electrodes are 0.1, 0.1, 0.3,0.6, 0.8, respectively.

5. Conclusion

This paper provides a number of insights that can help understand and design futuristic devices.

1. Experimental transport study showed that increasing FM electrode thickness did not allow the strong molecular coupling effect to produce the same orders of current suppression.
2. Experimental MFM study showed that the pillar-shaped MTJMSD, where FM electrodes were confined with the smallest region, produced a similar type of response. However, Cross junction-shaped MTJMSD with extended FM electrodes exhibited a significant difference in and around magnetic phases with time.
3. MCS study on cross junction shaped MTJMSD showed long FM electrodes possess different magnetic phases in an equilibrium state. The variety of phases coexisting magnetic phases increased with length.
4. MCS study showed that increasing thickness weakens the molecular coupling impact range. With increasing thickness, a gradient of magnetic properties appeared. The section of FM electrode away from the junction possessed disordered states.
5. MCS study showed that increasing FM electrode length for low thickness FM electrode did not alter critical molecular coupling strength.
6. Interestingly, critical molecular coupling strength for pillar-shaped MTJMSD (with no extended FM electrodes) was more than that of cross-junction-shaped MTJMSD.
7. MCS study showed that increasing thickness made it difficult to switch a device between high to low magnetic moment states. This result is of critical importance and suggests that experimental studies should focus on thin films. According to our experimental study, the critical thin film thickness is around 10 nm.

Declaration of competing interest

The authors declare that they have no known competing financial interests or personal relationships that could have appeared to influence the work reported in this paper.

Acknowledgement

We gratefully acknowledge the funding support from National Science Foundation (Contract #HRD- 1914751), and the Department of Energy/National Nuclear Security Agency (DE-FOA-0003945). Pawan thanks the University of Kentucky and Prof. Bruce Hinds for facilitating PhD work on molecular spintronics, for which OMC molecules were thankfully provided by Steve Holmes's group.

References

[1] L. Bogani, W. Wernsdorfer, Molecular spintronics using single-molecule magnets, Nat. Mater. 7 (3) (2008) 179–186.
[2] A.R. Rocha, V.M. Garcia-Suarez, S.W. Bailey, C.J. Lambert, J. Ferrer, S. Sanvito, Towards molecular spintronics, Nat. Mater. 4 (4) (2005) 335–339.
[3] A.N. Pasupathy, R.C. Bialczak, J. Martinek, J.E. Grose, L.A.K. Donev, P.L. McEuen, D.C. Ralph, The Kondo effect in the presence of ferromagnetism, Science 306 (5693) (2004) 86–89.
[4] J.R. Petta, S.K. Slater, D.C. Ralph, Spin-dependent transport in molecular tunnel junctions, Phys. Rev. Lett. 93 (13) (2004) 136601.
[5] P. Tyagi, Multilayer edge molecular electronics devices: a review, J. Mater. Chem. 21 (13) (2011) 4733–4742.
[6] E. Coronado, M. Clemente-León, J.R. Galán-Mascarós, C. Giménez-Saiz, C. J. Gómez-García, E. Martínez-Ferrero, Design of molecular materials combining magnetic, electrical and optical properties, J. Chem. Soc., Dalton Trans. (21) (2000) 3955–3961.
[7] N. Maciel, E. Marques, L. Naviner, Y. Zhou, H. Cai, Magnetic tunnel junction applications, Sensors 20 (1) (2020) 121.
[8] G.X. Miao, M. Munzenberg, J.S. Moodera, Tunneling path toward spintronics, Rep. Prog. Phys. 74 (2011) 36501.
[9] J.S. Moodera, J. Nassar, G. Mathon, Spin-tunneling in ferromagnetic junctions, Annu. Rev. Mater. Sci. 29 (1999) 381–432.
[10] S. Parkin, Spin-polarized current in spin valves and magnetic tunnel junctions, MRS Bull. 31 (5) (2006) 389–394.
[11] N. Prokopuk, K.A. Son, Alligator clips to molecular dimensions, J. Phys.-Condes. Matter. 20 (37) (2008) 374116.
[12] M. Gobbi, A. Pascual, F. Golmar, R. Llopis, P. Vavassori, F. Casanova, L.E. Hueso, C-60/NiFe combination as a promising platform for molecular spintronics, Org. Electron. 13 (3) (2012) 366–372.
[13] J.R. Heath, Molecular electronics, Annu. Rev. Mater. Res. 39 (2009) 1–23.
[14] P. Tyagi, D.F. Li, S.M. Holmes, B.J. Hinds, Molecular electrodes at the exposed edge of metal/insulator/metal trilayer structures, J. Am. Chem. Soc. 129 (16) (2007) 4929–4938.
[15] P. Tyagi, C. Riso, E. Friebe, Magnetic tunnel junction based molecular spintronics devices exhibiting current suppression at room temperature, Org. Electron. 64 (2019) 188–194.
[16] P. Tyagi, C. Riso, Magnetic force microscopy revealing long range molecule impact on magnetic tunnel junction based molecular spintronics devices, Org. Electron. 75 (2019) 105421.
[17] P. Tyagi, C. Riso, Molecular spintronics devices exhibiting properties of a solar cell, Nanotechnology 30 (49) (2019) 495401.
[18] P. Tyagi, E. Friebe, Large resistance change on magnetic tunnel junction based molecular spintronics devices, J. Magn. Magn Mater. 453 (2018) 186–192.
[19] D.F. Li, S. Parkin, G.B. Wang, G.T. Yee, R. Clerac, W. Wernsdorfer, S.M. Holmes, An S=6 cyanide-bridged octanuclear (Fe4Ni4II)-Ni-III complex that exhibits slow relaxation of the magnetization, J. Am. Chem. Soc. 128 (13) (2006) 4214–4215.
[20] D.F. Li, C. Ruschman, R. Clerac, S.M. Holmes, Ancillary ligand functionalization of cyanide-bridged S = 6 FeIII4NiII4 complexes for molecule-based electronics, Inorg. Chem. 45 (13) (2006) 7569.
[21] C.E. Inman, S.M. Reed, J.E. Hutchison, In situ deprotection and assembly of S-tritylalkanethiols on gold yields monolayers comparable to those prepared directly from alkanethiols, Langmuir 20 (2004) 9144–9150.
[22] L. Cheng, J.P. Yang, Y.X. Yao, D.W. Price, S.M. Dirk, J.M. Tour, Comparative study of electrochemically directed assembly versus conventional self-assembly of thioacetyl-terminated oligo(phenylene ethynlyene)s on gold and platinum surface, Langmuir 20 (4) (2004) 1335–1341.
[23] M. Ouyang, D.D. Awschalom, Coherent spin transfer between molecularly bridged quantum dots, Science 301 (5636) (2003) 1074–1078.
[24] S. Sanvito, Injecting and controlling spins in organic materials, J. Mater. Chem. 17 (42) (2007) 4455–4459.
[25] S. Sanvito, MOLECULAR SPINTRONICS the rise of spinterface science, Nat. Phys. 6 (8) (2010) 562–564.
[26] A.P. Weber, A.N. Caruso, E. Vescovo, M.E. Ali, K. Tarafder, S.Z. Janjua, J. T. Sadowski, P.M. Oppeneer, Magnetic coupling of Fe-porphyrin molecules adsorbed on clean and c(2 x 2) oxygen-reconstructed Co(100) investigated by spin-polarized photoemission spectroscopy, Phys. Rev. B 87 (18) (2013) 184411.
[27] D. Chylarecka, T.K. Kim, K. Tarafder, K. Muller, K. Godel, I. Czekaj, C. Wackerlin, M. Cinchetti, M.E. Ali, C. Piamonteze, F. Schmitt, J.P. Wustenberg, C. Ziegler, F. Nolting, M. Aeschlimann, P.M. Oppeneer, N. Ballav, T.A. Jung, Indirect magnetic coupling of manganese porphyrin to a ferromagnetic cobalt substrate, J. Phys. Chem. C 115 (4) (2011) 1295–1301.
[28] A. Candini, V. Bellini, D. Klar, V. Corradini, R. Biagi, V. De Renzi, K. Kummer, N. B. Brookes, U. del Pennino, H. Wende, M. Affronte, Ferromagnetic exchange coupling between Fe phthalocyanine and Ni(111) surface mediated by the extended states of graphene, J. Phys. Chem. C 118 (31) (2014) 17670–17676.
[29] K. Park, H.S. M, Exchange coupling and contribution of induced orbital angular momentum of low-spin Fe3+ ions to magnetic anisotropy in cyanide-bridged Fe2M2 molecular magnets: spin-polarized density-functional calculations, Phys. Rev. B 74 (2006) 224440.
[30] A. McCaskey, Y. Yamamoto, M. Warnock, E. Burzuri, H.S.J. van der Zant, K. Park, Electron-vibron coupling effects on electron transport via a single-molecule magnet, Phys. Rev. B 91 (12) (2015).
[31] P. Tyagi, C. Riso, U. Amir, C. Rojas-Dotti, J. Martínez-Lillo, Exploring room-temperature transport of single-molecule magnet-based molecular spintronics

devices using the magnetic tunnel junction as a device platform, RSC Adv. 10 (22) (2020) 13006–13015.
[32] P. Tyagi, C. Baker, C. D'Angelo, Paramagnetic molecule induced strong antiferromagnetic exchange coupling on a magnetic tunnel junction based molecular spintronics device, Nanotechnology 26 (2015) 305602.
[33] P. Tyagi, H. Brown, A. Grizzle, C. D'Angelo, B.R. Dahal, Molecular coupling competing with defects within insulator of the magnetic tunnel junction-based molecular spintronics devices, Sci. Rep. 11 (1) (2021) 1–13.
[34] X. Hao, J.S. Moodera, R. Meservey, Spin-filter effect of ferromagnetic Europium sulfide tunnel barriers, Phys. Rev. B 42 (13) (1990) 8235–8243.
[35] S. Joo, K. Jung, K. Jun, D. Kim, K. Shin, J. Hong, B. Lee, K. Rhie, Spin-filtering effect of thin Al2O3 barrier on tunneling magnetoresistance, Appl. Phys. Lett. 104 (15) (2014) 152407.
[36] J.G. Simmons, Generalized formula for electric tunnel effect between similar electrodes separated by a thin insulating film, J. Appl. Phys. 34 (6) (1963) 1793.
[37] P. Tyagi, E. Friebe, C. Baker, Addressing the challenges of using ferromagnetic electrodes in the magnetic tunnel junction-based molecular spintronics devices, J. Nanoparticle Res. 17 (11) (2015) 452.
[38] S. Yuasa, D. Djayaprawira, Giant tunnel magnetoresistance in magnetic tunnel junctions with a crystalline MgO (0 0 1) barrier, J. Phys. D Appl. Phys. 40 (21) (2007) R337.